J Mater Sci (2007) 42:7123–7128
DOI 10.1007/s10853-007-1531-z

Evolution of microstructures and phases of Al–Mg alloy under 4 GPa high pressure

Z. J. Wei · Z. L. Wang · H. W. Wang · L. Cao

Received: 13 June 2006 / Accepted: 16 January 2007 / Published online: 5 May 2007

Abstract Optical microscope (OM), energy dispersive X-ray (EDX) analysis, differential scanning calorimetry (DSC), X-ray diffraction (XRD) and transmission electron microscope (TEM) were applied to investigate the solidification microstructures and phases of Al–9.6 wt.% Mg alloy which solidified under 4 GPa high pressure with the melting temperature 1,153 K. Fine dendritic microstructures were obtained, and the second dendritic arm spacing reduced. Area fraction of the primary α-Al phase increased and that of the second phase decreased. In addition, the solid solubility of Mg in α-Al phase increased. The lattice constant of α-Al phase increased. Specially, the new double phase regions (α-Al′ + Al_xMg_y) formed besides a small amount of Al_3Mg_2 phases under high pressure. The Al_xMg_y phase presented a mean size of about 20 nm, and had the hexagonal structure with the lattice constant of a = 0.288 nm, c = 0.8165 nm probably. Wherein the lattice constant of α-Al′ phase differed from that of α-Al phase greatly. Moreover, evolution mechanism of microstructures and phases under 4 GPa high pressure was discussed.

Introduction

Pressure is, like temperature, a basic thermodynamic variable which can be used to transport matter from one state to another [1]. Therefore, there has been more and more application of the high pressure technology in materials science and engineering in recent years. First, it is used to synthesize some metastable materials with special properties such as diamond, amorphous and nanocrystalline [2–4]. Second, it can improve the properties of the alloy. Finally, high pressure technology provides a method to create novel materials not accessible by other techniques [1]. For example, Yu [5] prepared high-T_c Superconductor $AuBa_2Ca_{n-1}Cu_nO_{2n+3}$ (n = 3, 4) under high pressure, and Eremets et al. [6] studied the miniature high pressure cells for high magnetic field applications. However, up to now, little attention is paid to effects of high pressure on solidification process of the common alloy both in practical application and theory. Great changes must happen to high pressure solidification process because of influences of pressure on thermodynamics and kinetics of crystallization process [7]. The phase diagram is shifted to the upper right direction when Al–26.6 wt.% Si alloy solidified under high pressure (5.5 GPa, 1,473 K) [8], and the primary phase is transformed from β phase to (α + β) phases. Moreover, the solid solubility of Si in α-Al and Al in β phase increased.

Al–Mg alloy has a wide range of application because of its excellent mechanical property and corrosion resistant as a structural material. However, there was very little work to be done about high pressure solidification of Al–Mg alloy. Therefore, Al–9.6 wt.% Mg alloy is chosen to study its evolution of the microstructures and the phases under high pressure in the paper. Some new phenomena appeared in the experiment were discussed to some extent. At the same time, it is very important for expanding the range of solidification theory.

Experimental

The alloy with nominal composition Al–12 wt.% Mg was produced by conventional casting from 99.97% pure Al

Z. J. Wei · Z. L. Wang (✉) · H. W. Wang · L. Cao
School of Materials Science and Engineering, Harbin Institute of Technology, Harbin 150001, China
e-mails: weizj@hit.edu.cn; wzlhit@gmail.com

and Mg. Chemical analysis of the alloy showed that Mg content was 9.6 wt.%. Typical total impurity content was about 0.003 wt.% (mainly Si). Metal mold (45 steel) was used in the experiment. KCl39% + $MgCl_2$61% (flux) was chosen to prevent the oxidation of the melt during melting process. The castings were machined into the high-pressure samples with the size of ∅ 5 × 5 mm. The high-pressure equipment used in the present experiment was a CS-1B type hexahedral hydraulic ram.

In the experimental, the sample was put into a boron nitride (BN) crucible that was inserted in a graphite furnace. The electrical contacts between the furnace and the power supply were made of steel dies. Pyrophillite was used as encapsulant and transmitting mediums. The pressure was slowly increased up to 4 GPa, and then the sample was heated up to the target value (1,153 K). The sample was kept at the target pressure and the target temperature for 6 min to make the pressure well distributed and steady in the pressure cell. After that, the sample was cooled down to room temperature by switching off the power supply. Finally, the sample was taken out for testing after pressure relief.

After the sample was polished and etched using 0.5% HF + 99.5% H_2O solution, investigation on the microstructure was carried out on OLYMPUS optical microscope. The composition of the phases was measured by energy dispersive X-ray microanalysis (EDX) in JEOL S-570 scanning electron microscope (SEM), and the electron beam accelerating voltage was 25 kV. To obtain accurate EDX results, Standardless EDAX ZAF quantification method was used to perform elemental microanalysis. Moreover, the phase transformation of the alloy under different pressures was measured by differential scanning calorimetry (DSC) (Perkin–Elmer Pyris-I) with a heating rate of 20 K/min under a flowing argon atmosphere. And the DSC data were treated with the Pyris data analysis program supplied by Perkin–Elmer Company. X-ray diffraction (XRD) was conducted on a Rigaku D/max-RB X-ray diffractmeter with monochromatic CuK_α radiation. Specimens for transmission electron microscope (TEM) were first sliced to 300 μm by sparking and then mechanically ground to a thickness of 50 μm. The grinding was followed by the standard ionic thinning (Gatan Model 691 PIPS) in 25% nitric acid and 75% methanol solution. The selected area diffraction (SAD) studies were performed on a Philips CM12 microscope with the acceleration voltage 120 kV. The solidification temperature of the alloy was tested by PtRh-Pt thermal couple, which reached the sample through the pyrophyllite and the graphite furnace as well as BN crucible. The cooling curve of the alloy, recorded by X-Y recorder when the alloy solidified under different pressures, was about 250–300 K/s by calculation at 4 GPa, and 100 K/s or so under normal pressure.

Results and discussions

Microstructure and chemical composition of the phase

Figure 1a represents the microstructures of Al–9.6 wt.% Mg alloy that solidified under normal pressure. The alloy contains the coarse dendritic primary α-Al and the interdendritic β-Al_3Mg_2 phase. However, at 4 Gpa the dendrite microstructures are refined apparently, as shown in Fig. 1 c, for example, the second dendrite arm spacing decreases from 14 μm of normal pressure to 12 μm of 4 GPa. As shown in Fig. 1b and d, the morphology of the interdendritic phase also changes from plate to graininess, accompanied by a great decrease in the size. The average size of β phase is 10–45 μm under normal pressure, while it is just about 5 μm at 4 GPa. Correspondingly, the area fraction of the second phase in Al–Mg alloy reduces from 19.1 to 6.9%. In addition, Mg concentration in α phase is 7.74 wt.% under normal pressure; however, it increases up to 11.58 wt.% at 4 GPa. That is to say, α-Al solid solution is supersaturated under high pressure. And Mg concentration in the second phase decreases from 36.19 to 26.12 wt.% with the pressure increasing. Therefore, the second phase formed at 4 GPa needs to be confirmed further.

Effects of high pressure on the second dendritic arm spacing can be expressed by [9]

$$d_2 = Av^{-\frac{1}{3}} \tag{1}$$

$$A = \left(\frac{16\Delta T_S \sigma T_L D_L}{\rho_S \Delta H_m m_L C_L (1 - K_0)}\right)^{\frac{1}{3}}, \tag{2}$$

where d_2 is second dendrite arm spacing, v is the cooling rate, ΔT_S is the ranges of temperature of non-equilibrium solidification, σ is the surface curvature of the dendrite, T_L is the temperature of the liquidus (K), D_L is the diffusion coefficient of the solute in the liquid (m^2/s), ρ_S is the density of the solid (kg/m^3) ΔH_m is the latent of heat of fusion (J/g), m_L is the liquidus slope, C_L is the equilibrium concentration of the liquid phase, and K_0 is the equilibrium partition ratio of the solute. Here superscript P represents high pressure, and others represent normal pressure. It is found that all parameters vary under high pressure according to Eq. 1 and Eq. 2, however, variations of D_L, T_L and m_L are more obvious. Relation of diffusion coefficient (D_L) and pressure has been given in [10]

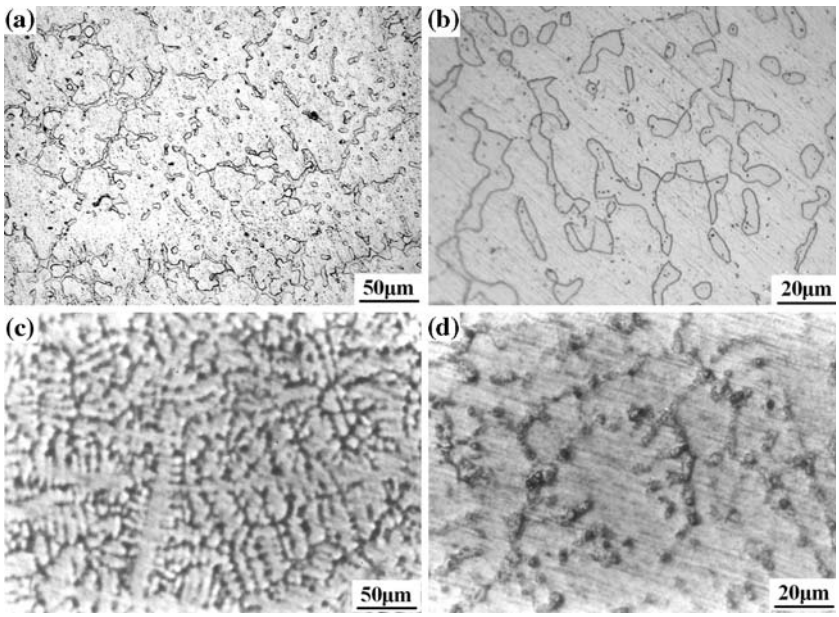

Fig. 1 Microstructures of Al–9.6 wt.% Mg alloy solidified under different pressures (**a**), (**b**) normal pressure; (**c**), (**d**) 4 GPa

$$D = RT\delta^{-1}\eta^{-1} = RT\delta^{-1}\eta_0^{-1}e^{-(PV_0/RT)}, \quad (3)$$

where R is the gas constant, T (K) is the temperature of the melt, δ (m) is the distance of free path of the atom, η_0 (Pa s) is the viscosity under atmosphere conditions at the same temperature, and V_0 (m^3/mol) is the original volume of the liquid phase. Then Eq. 3 can be deduced as

$$D_L^P/D_L = e^{(1.013\times10^5-p)V_0/RT} = e^{-PV_0/RT}. \quad (4)$$

It is estimated that V_0 equaled to 1.176×10^{-5} m^3/mol near the melting point of Al–9.6Mg alloy according to the literature [9]. So $D_L^P/D_L = 6.78 \times 10^{-3}$ is achieved under 4 GPa high pressure. It can be seen that diffusion coefficient decreases three orders at 4 GPa, and the changes of T_L and m_L are small compared with the diffusion coefficient. So A is determined mainly by diffusion coefficient D_L. According to Eq. 1, increasing pressure (GPa level) causes the second dendrite arm spacing to decrease with the same cooling rate. In addition, the cooling rate under high pressure is greater than that of normal pressure in the light of the experimental results, which results mainly from increasing heat transfer rate under high pressure [11]. These also contribute to the decrease of the second dendrite arm spacing to some extent.

Effects of high pressure on the area fraction of the second phases can be explained as the following. Solid solubility of Mg in α-Al phase increases owing to the decrease of the diffusion coefficient and the increase of cooling rate. Moreover, the melting point of Al–Mg alloy under high pressure is given by the well-known Clapeyron equation [12]

$$\frac{dT_P}{dP} = -\frac{T_m\Delta V}{\Delta H}, \quad (5)$$

where P is pressure, T_m is the melting point of the alloy, ΔV is the volume change during solidification, and ΔH is the latent heat of fusion, taking it as positive during exothermic reaction, or else as negative. From Eq. 5, high pressure results in the increase of the melting point of Al–Mg alloy since its volume decreases during solidification process. Namely, the temperatures of the liquidus and the solidus increase under high pressure. Moreover, solid solubility of Mg in α-Al phase increases at 4 GPa. This suggests that high pressure expands α-Al phase field, and the corresponding solid solubility limit increases. As a result, under the condition of high pressure, phase diagram moves to the direction of high temperature and high Mg content. The area fraction of α-Al phases increases and that of the second phases decreases on the basis of lever principle of the phase diagram.

Effects of high pressure on the second phase

For a better understanding of effects of high pressure on the solidification process, DSC experiment was performed on the samples that solidified under normal pressure and high pressure, respectively. DSC curves of Al–9.6 wt.% Mg alloy solidified under different pressures are presented in Fig. 2. It is noted that there are two melting peaks under normal pressure: the first one (725–741 K) results from the eutectic (α-Al + Al_3Mg_2) reaction based on the Al–Mg phase diagram [13], and the second one is caused by melting of α-Al phases completely. While, at 4 GPa there is a new melting peak appears which overlaps the first peak

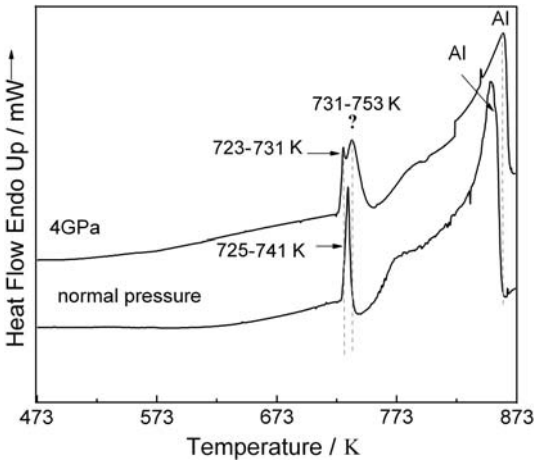

Fig. 2 DSC curves for Al–9.6 wt.% Mg alloy solidified under different pressures. Heating rate is 20 K/min

(723–731 K), and its melting temperature is in the range of 731–753 K. It indicates that a new phase formed when applying high pressure on the crystallization process of the alloy. However, when high-pressure sample after DSC experiment is remelted; the new melting peak (731–753 K) disappears and a eutectic reaction peak (724–734 K) occurs again, shown in Fig. 3. It suggests that the new phase under high pressure is metastable. In view of the new melting peak in DSC curves, we are going to proceed to XRD and TEM tests to identify the new phase under high pressure.

Figure 4 shows XRD pattern of Al–9.6 wt.% Mg alloy solidified under different pressures. It reveals the presences of α-Al and β-Al_3Mg_2 phase under normal pressure. While, at 4 Gpa the diffraction peaks of β phases disappear and only those of α-Al phases can be observed, indicating that the volume fraction of β phases is small. At the same time, it is found that the diffraction peaks of α-Al phase is shifted to lower 2θ up to 0.5–0.9 degree, meaning that the lattice constant of α-Al phase increases when the alloy solidified at 4 GPa. It is calculated that the lattice constant of α phase is 0.40896 nm under normal pressure based on XRD data, and at 4 GPa it increases up to 0.411 nm. It is known that the lattice parameter of aluminum expands by approximately 0.005×10^{-10} m for every 1%Mg [14]. Depending on this rule, the lattice constant is 0.40916 nm under normal pressure and 0.41069 nm at 4 GPa, respectively, which agrees with those obtained from XRD data basically. Therefore, the lattice dilation under high pressure arises mainly from the increase of Mg concentration in α phase.

In TEM observations, two kinds of phases (the gray and the black ones) are found in the sample when Al–Mg alloy solidified at 4 GPa, as shown in Fig. 5a and c. The sizes of the phases are between 90 and 240 nm. Particularly, it is found that the gray phases consist mostly of Al matrix and fine particles after magnification, and the average size of the particles is 20 nm, shown in Fig. 5b. It is well known that the crystals region or other characteristic length being in the range of nanometer order (less than 100 nm) is defined as nanophase materials or nanometer-structured materials [14]. Therefore, it is a very important discovery that the nanometer-size phase is formed in Al–9.6 wt.% Mg alloy when applying pressure (4 GPa) during solidification process. Figure 5d shows SAD pattern taken from area ''A'' as indicated in Fig. 5c. It has F.C.C structure and the lattice constant is about 2.818 nm, which are in agreement with the lattice constant (2.8239 nm) of Al_3Mg_2 phase [13]. Figure 5e and f represent SAD patterns of the gray phase from area ''B'' and ''C'' as indicated in Fig. 5c, respectively. From Fig. 5e, it is very possible that the particles are hexagonal structure and the lattice constant is about a = 0.288 nm, c = 0.8165 nm by calibration. We consider the phase to be a new phase since its lattice constant is not the known ones composed of Al and Mg,

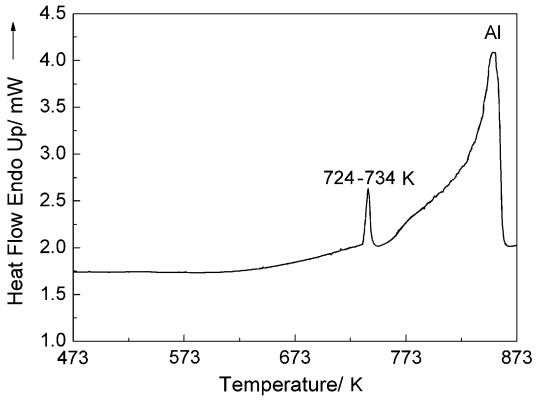

Fig. 3 DSC curve of repeating the DSC heating experiment in Al–9.6 wt.% Mg alloy

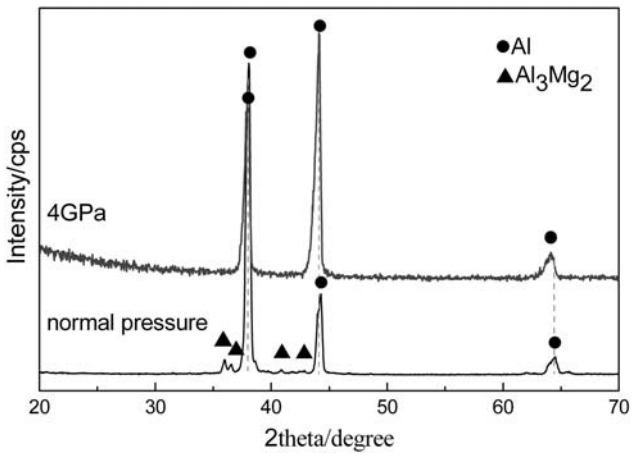

Fig. 4 XRD spectrum of Al–9.6 wt% Mg alloy solidified under different pressures

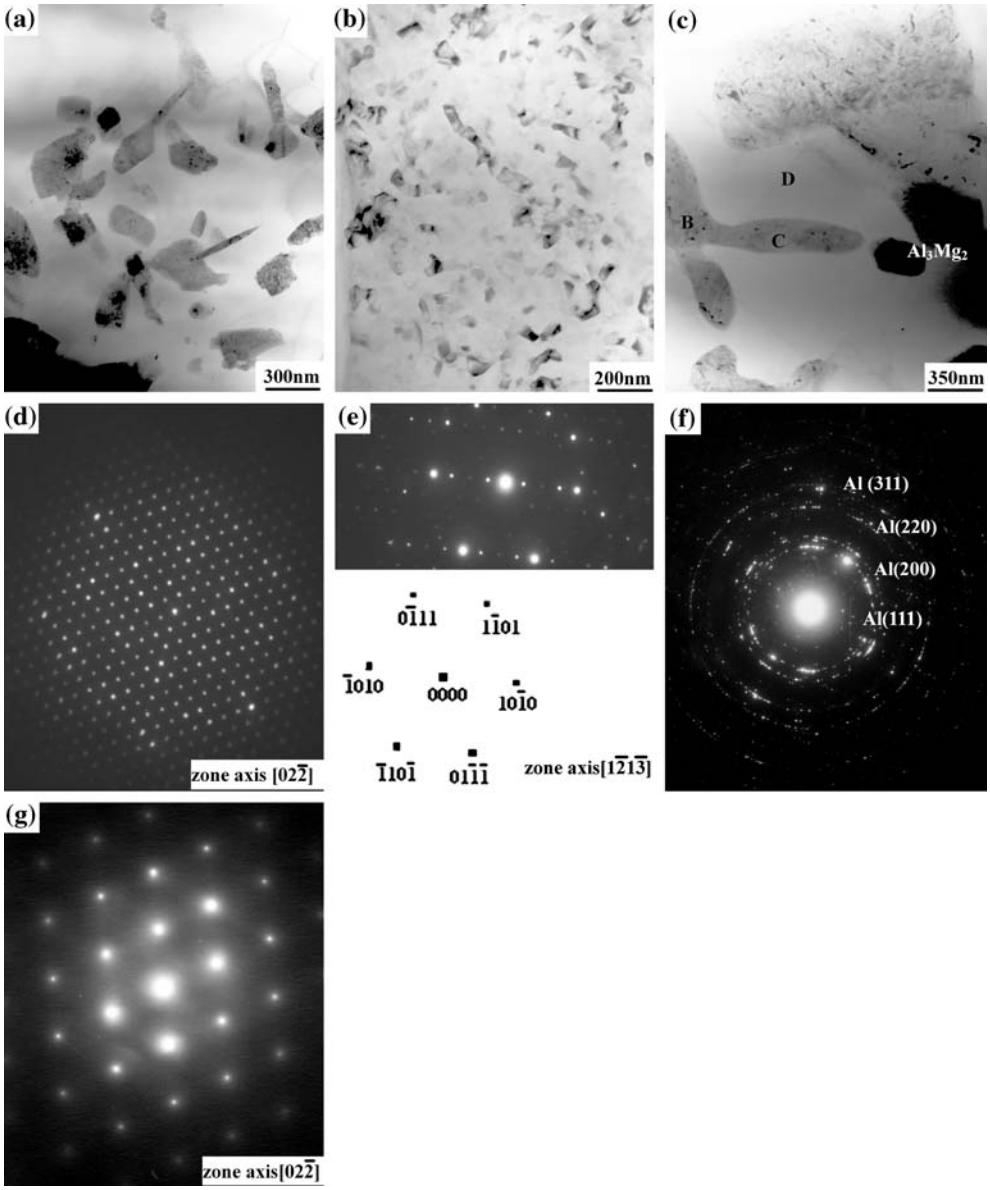

Fig. 5 TEM photographs of Al–9.6 wt.% Mg alloy when solidified at 4 GPa. (**a**) and (**c**) are morphology of the second phase; (**b**) is micro-morphology of the magnified gray phase; (**d**) is SAD pattern from area ''A'' indicated in (**c**); (**e**) and (**f**) are SAD patterns from area ''B'' and ''C'' indicated in (**c**), respectively; (**g**) is SAD pattern of α-Al matrix indicated in area ''D''

and the new phase is a metastable phase in the light of the previous analysis. Here the phase is symbolized by Al_xMg_y phase. Figure 5f shows the SAD pattern of α-Al phase with the axis zone [0, 2, –2] and the lattice constant 0.4007 nm, which is symbolized as α-Al′ to distinguish with α-Al phase (Al matrix). The diffraction pattern of α-Al phase shown in area ''D'' is displayed in Fig. 5g, and its lattice constant is 0.415 nm much greater than that of α-Al′ phase. So we deduce that Al_xMg_y phases are precipitated from Mg-rich regions of the alloy, which leads to the decrease of Mg concentration in Mg-rich regions extremely, consequently, the lattice constant of α-Al′ phase decreases much in comparison with that of α-Al phase. Therefore, the gray phases are a double phase regions which are composed of α-Al′ phase and Al_xMg_y phase with nanometer size. It is an interesting phenomenon under high pressure solidification conditions. So the new melting peak in the range of 731–753 K in DSC curves should be caused by the melting of (Al_xMg_y) phase, and its melting point is just a little larger than that of Al_3Mg_2 phase. Therefore, we make the conclusion that there is a new metastable phase having hexagonal structure precipitated from Mg-rich regions probably, with the lattice constant $a = 0.288$ nm, $c = 0.8165$ nm. Furthermore, there is still a few Al_3Mg_2 phase formed when Al–9.6 wt% Mg alloy solidified at 4 GPa. Certainly, the crystal structure of the metastable phase at 4 GPa needs to be studied further in the future work.

Formations of the new phase with hexagonal structure are correlated with effects of high pressure on microscopic

structure of the melt. It has been reported in the literature [15] that high pressure shortens the interatomic distance and contributes to formation of the compact phase. This is one of the reasons why the hexagonal structure Al_xMg_y can be obtained under high pressure. In addition, diffusion coefficient of the atoms in melt decreases three orders at 4 GPa according to the previous results, which means that the solute atoms ahead of the solid/liquid interface are not easy to diffuse away, resulting in more and more solutes are accumulated at the interdendritic parts and the Mg-rich regions formed. Parts of Mg-regions reach the composition of Al_3Mg_2 phase and the stable phases produced; others get unstable with the temperature decreasing and precipitate from some of Mg-rich regions as a metastable phase (Al_xMg_y). As a result, double phase regions (α-Al′+Al_xMg_y) are found in TEM observation. Therefore, the interdendritic phases shown in Fig. 1d should be the mixed phases including α-Al′, Al_xMg_y and Al_3Mg_2.

It is well known that the size dimension of the phase is connected with growth rate. The growth rate of the crystal under normal pressure is given as [12]

$$R = av_{\text{net}} = av_0 e^{-(\Delta G_b/kT)}(1 - e^{-(\Delta G_m/kT)}), \quad (6)$$

where a is the amount the interface advance when a molecule is added, v_{net} is the net jump frequency across the interface, ΔG_b is the activation energy that needs to surmount for an atom transport from the liquid to the solid, k is Boltzmann constant, ΔG_m is the free energy change per atom for the liquid–solid transition [9]

$$\Delta G_m = \frac{\Delta H_0 \Delta T_k}{T_m}. \quad (7)$$

Now, substituting Eq. 7 into (6) yields

$$R = av_0 e^{-(\Delta G_b/kT)}(1 - e^{-(\Delta H_0 \Delta T_k/kTT_m)}). \quad (8)$$

Taking $R(P)$ as growth rate under high pressure and $R(P_0)$ under normal pressure, diffusion of the atoms plays the major role during the growth process of the crystal, here high pressure has little effects on other parameters, so the following expression is achieved:

$$\frac{R(P)}{R(P_0)} = e^{[\Delta G_b(P_0) - \Delta G_b(P)]}. \quad (9)$$

We know that pressure can restrain the diffusion of atoms from the above analysis. These increase the activity energy of the crystal growth, so that $\Delta G_b(P_0) < \Delta G_b(P)$. Thus it can be deduced that $R(P) < R(P_0)$. So it is concluded that pressure suppresses the crystal growth, which leads to the formation of nanometer-size Al_xMg_y phase in the experiment. Furthermore, high pressure increases the cooling rate of the alloy in the experiment, which causes the growth rate of the crystal to reduce, too. However, the order of magnitude that the cooling rate increases is much less than that of diffusion coefficient decreases based on the previous results. Therefore, high pressure is the major factor which contributes to nanometer-length microstructure.

Conclusions

(1) When Al–9.6 wt.% Mg alloy solidified at 4 GPa, the dendrite microstructures are refined. The area fraction of the second phase decreases and that of the primary α-Al phase increases. Mg concentration in α-Al phase rises from 7.74 wt.% under normal pressure to 11.58 wt.% at 4 GPa. Correspondingly, the lattice constant of α-Al phase changes from 0.40896 to 0.411 nm.

(2) New double phase regions (α-Al′ + Al_xMg_y) are obtained in the alloy at 4 GPa, wherein the Al_xMg_y phase is a metastable phase. It has hexagonal structure with the lattice constant of a = 0.288 nm, c = 0.8165 nm probably. And the lattice constant of α-Al′ is much less than that of α-Al phase. The size of the Al_xMg_y phase is in the range of nanometer order. In addition, there is still a small amount of Al_3Mg_2 phase at 4 GPa.

References

1. Schilling JS (1998) J Phys Chem Solids 59(4):553
2. Choudhary D, Bellare J (2000) Ceram Int 26:73
3. Fukunaga O, et al (1999) Diamond Related Mater 8:2036
4. Hu ZQ, Ding BZ, Zhang HF, et al (2001) Sci Technol Adv Mater 2:41
5. Yu S, Kopnin EM, Takayama-Muromachi E (2003) Sci Technol Adv Mater 4:277
6. Eremets MI, Struzhkin VV, Utjuzh AN (1995) Physica B 211:369
7. Li D-J (1983) Phase transformation mechanism of the metastable phase under high pressure. Institute of Metal Research Academy of Sciences, Shenyang, p 46, 74, 96 (in Chinese)
8. Zhang G, et al (1999) Acta Metall Sin 35(3):285 (in Chinese)
9. Hu H (1985) Metal solidification. Metallurgical Industry Press, Peking, p 213 (in Chinese)
10. Batashef AE (1987) Crystallization of metal and alloys at pressure. Harbin Institute of Technology Publisher, Harbin, p 23, 21 (in Chinese)
11. Han YS, Kim DH, Lee HI (1994) Scrip Metall Mater 31:1623
12. Flemings MC (1974) Solidification processing. The Maple Press Company, p 266, 305
13. Mondolfo LF (1976) Aluminum alloys: structure and properties. © Butterworth & Co Publishers Ltd, London, p 313, 312
14. Cahn RW (1990) Nature 348:389
15. Zhicheng Q (1991) Chinese J High Pressure Phys 5(3):193